



Short Communication

Semi-solid wire-feed additive manufacturing of AlSi7Mg by direct induction heating



Lukas Englert*, Alexander Klumpp, Antonia Ausländer, Volker Schulze, Stefan Dietrich

Karlsruhe Institute of Technology, Institute for Applied Materials (IAM-WK), Engelbert-Arnold-Straße 4, Karlsruhe 76131, Germany

ARTICLE INFO

Keywords:

Wire-feed additive manufacturing
 Induction heating
 AlSi7Mg
 Micro-computed tomography
 Semi-solid processing

ABSTRACT

In this study, a novel process is presented in which direct induction heating with frequencies in the MHz range is used for the wire-feed additive manufacturing of the alloy AlSi7Mg. The high frequency of 1.5 MHz enables processing of 1.2 mm diameter wires without the need for indirect heating via a nozzle. The feasibility of the process is proven by the experimental identification of a proper process window regarding the influential parameters such as the distance between inductor and substrate, induction power and wire feed rate for the fabrication of single layers. Furthermore, a strategy for the successful fabrication of multi-layered cubes is developed. The microstructure of the cubes exhibits a characteristic variation along the build direction. Micro-computed tomography is used to reveal defects like lack of fusion and spherical pores in test cubes. The presented results are used to derive possible process improvements, which will allow the novel process to be used as a fast and powder-free alternative metal additive manufacturing route in future.

1. Introduction

During the last decades, wire-feed additive manufacturing (WFAM) has become a powerful process for additive manufacturing of metallic structural components, such as parts made of Aluminium and its alloys [1,2] as well as for example 316L [3] or NiTi shape memory alloy [4]. The underlying processes are usually laser-based, arc welding-based or electron beam-based, and commonly regarded as environmentally friendly, since they comprise a high degree of material and energy efficiency. Compared to powder bed fusion processes part quality and accuracy are relatively poor, although approaches to increase accuracy of WFAM are currently under research [5]. However, WFAM can advantageously be used to build large parts of moderate complexity in reasonable time without the difficulty of handling powder and a high material usage efficiency [1].

During recent years, interest toward applying induction heating to additive manufacturing has arisen [6–11], as the process is well understood, precise and flexible [12,13]. Thus, several suggestions for its usage in the context of WFAM have been made. Sun and co-workers [7,8] recently proposed a laser-assisted high frequency ($750 \text{ kHz} < f < 1150 \text{ kHz}$) induction cladding process for the strengthening of stainless steel AISI 316L by wire-feed surface deposition of Inconel 625. Induction heating was used to melt the wires, while an additional laser was used to pre-heat the substrate. The authors could show that Inconel 625 coatings can be deposited properly, both as single- and multi-layers by

means of induction melting. They also emphasised that incomplete fusion may occur if either laser or induction power are too low, indicating that pre-heating is a necessary condition for successful application of the process.

Although Hascoët and co-workers formulated the idea of using induction heating for WFAM [9], the proposed coil did not allow deposition of beads side by side. In their combined experimental-numerical study on stainless steel 316L, the authors showed that induction heating may be used both to melt the wire and to actively pre-heat the substrate with the electromagnetic stray field. Wires were melted directly, i.e. without the usage of a nozzle. Results indicate a rather narrow process window regarding feed rates and induction power for proper material deposition. While a too large feed rate may prevent the wire from melting, excessively low feed rates may cause molten metal to stay on top of the coil due to Lorentz' force. Yet, the concept of the process was proven to be successful by multi-layer deposition of single tracks.

The idea of induction melting in WFAM was then only recently adapted by Sharma and co-workers, who presented an approach for Al-based alloys 4043 (AlSi5) [10] and 5356 (AlMg5) [11]. In their studies, electromagnetic induction with a power of 1 kW and a frequency of 100 kHz was used to heat a cast iron nozzle to temperatures around 580 °C, and by this means, to transfer wires of the applied Al-alloys with a diameter of 1.6 mm indirectly to the semi-solid state. Confirming earlier results [9], they found the distance between inductor and substrate to be crucial for the temperature evolution and the print results. Due to

* Corresponding author.

E-mail address: lukas.englert@kit.edu (L. Englert).

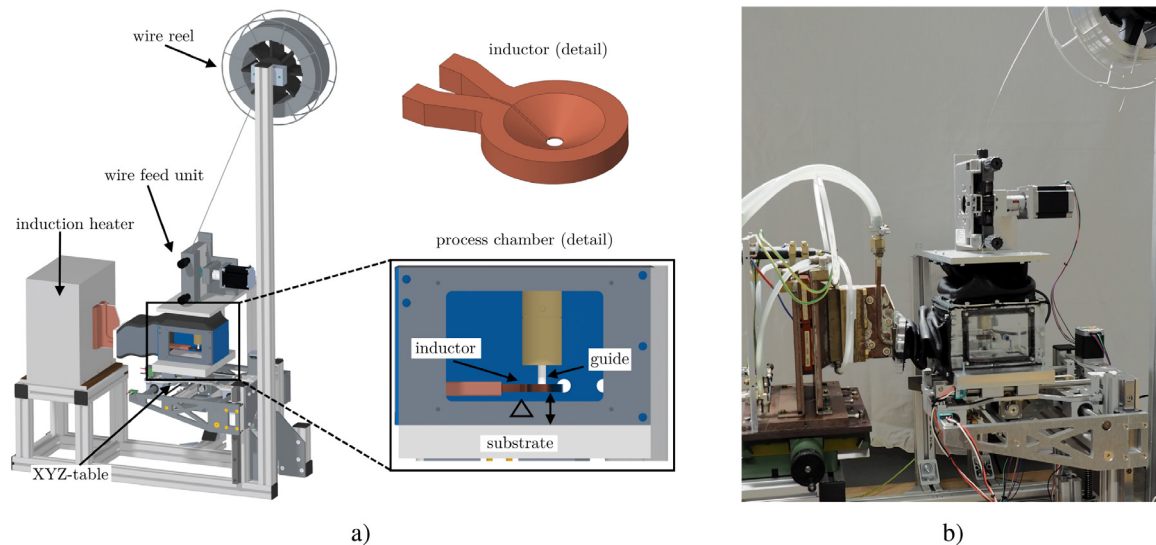


Fig. 2. Inductive-additive manufacturing setup: a): CAD rendering. b): Photograph of the fabrication setup.

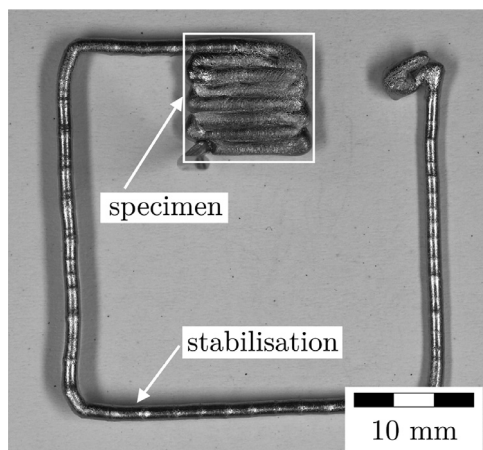


Fig. 3. Process and workpiece stabilisation using "scrap rectangle".

Process description

For the present study, substrate plates of $50 \times 50 \text{ mm}^2$ and a thickness of 2 mm were used. The plates were made of Al 6061 sheet and mounted to the XYZ-table with screws. In contrast to processes which apply heated nozzles, the present process is based on direct inductive wire heating. This means that the initial wire tip position has to be reproducible for each build job and that the onset of wire feed has to coincide precisely with the initiation of inductive power input. To achieve a steady state of the system at the beginning of each build job, the process was initiated by generating a scrap rectangle ($30 \times 30 \text{ mm}$) around the part to be manufactured. This is shown in Fig. 3. By this means, both the process and the mechanical stability are improved prior to fabricating the actual workpiece.

No pre-heating of the substrate plates was applied, since the evaluation of the feasibility of pure inductive WFAM was one of the main goals of the present study. A video of the system fabricating a cube specimen with removed inert gas chamber is included in the supplementary material.

2.3. Test plan and specimens

The present study followed a two-step experimental procedure. The first step was to facilitate the fabrication of single-layer specimens by

finding the range of feasible combinations of the main process parameters "induction power" (P_1), "feed rate" (v_s) and "distance inductor-substrate" (Δ). The second step was to adapt the most appropriate parameter set for the manufacturing of a multi-layer part. The inductor frequency was kept constant for all experiments at $f_i \approx 1.5 \text{ MHz}$.

2.3.1. Single-layer experiments

Single-layers of AlSi7Mg deposited with different process parameters led to different fabrication results concerning the quality of the layer. By optical evaluation of the fabrication results a process window was identified using three categories, neglecting the gradual transition between them:

1. Type I: Suitable semi-solid deposition with proper shape formation of the layer. Energy input and deposition temperature are appropriate. Additionally, points denoted with "Type I*" label suitable semi-solid deposition of the wire but poor shape formation of the layer.
2. Type II: Unsuitable drop formation due to full melting of the wire. Energy input is too high.
3. Type III: Breakage of wires due to insufficient heating of the wire. Energy input and deposition temperature are too low.

Exemplary fabrication results of the three outlined categories are shown in Fig. 4.

Single-layer experiments were performed for inductor-substrate distances Δ of 5 mm and 12 mm. To identify the process window, the inductor power P_1 was varied between 10 kW and 12.5 kW and the feed velocity v_s was varied between 500 mm/min and 2000 mm/min. Since high (low) induction power and slow (fast) feed velocity heated the wire too much (too little), experiments were defined in an iterative way after identifying the process boundaries to optimally define the process window. The line spacing and layer height was set to 1.2 mm, assuming that the shape of the wire does not change due to the deposition. The feed velocities 500 mm/min and 2000 mm/min correspond to approximate deposition rates of $9.4 \text{ mm}^3/\text{s}$ ($\sim 0.025 \text{ g/s}$) and $37.7 \text{ mm}^3/\text{s}$ ($\sim 0.1 \text{ g/s}$), respectively.

2.3.2. Multi-layer parts

For each P_1 setting investigated, the most promising combination of v_s and Δ in terms of visual appearance and geometric quality was selected for the generation of multi-layer cubes. They are shown in Table 2 as specimens S1, S2 and S3.

Despite the positive results of single-layer deposition, none of the selected initial single-layer parameter sets could be applied successfully to

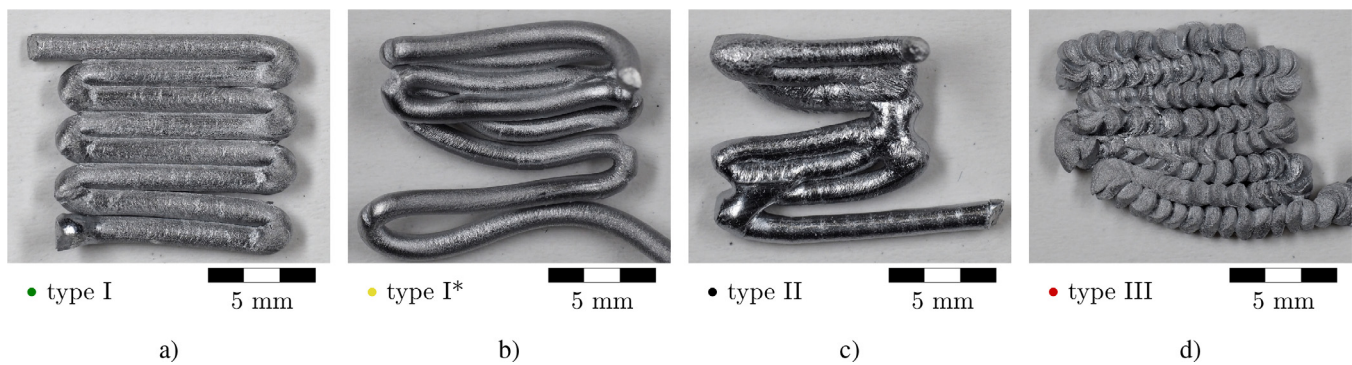


Fig. 4. Single-layer specimens produced with $P_1 = 10$ kW resulting in type a): I ($v_s = 900$ mm/min) c): II ($v_s = 800$ mm/min) and d): III ($v_s = 1000$ mm/min) fabrication results at $\Delta = 5$ mm. b): Type I* result, proper semi-solid deposition with poor shape of the layer ($v_s = 1100$ mm/min, $\Delta = 12$ mm).

Table 2

Parameter variation of P_1 and v_s for fabrication of multi-layer parts.

Specimen	Layer no.	=	1	2	3	4	5	6	7	8	9
S1	P_1 in kW	=					10 (const.)				
	v_s in mm/min	=					900 (const.)				
	Δ in mm	=					5 (const.)				
S2	P_1 in kW	=					11.25 (const.)				
	v_s in mm/min	=					1100 (const.)				
	Δ in mm	=					5 (const.)				
S3	P_1 in kW	=					12.50 (const.)				
	v_s in mm/min	=					1400 (const.)				
	Δ in mm	=					5 (const.)				
S4	P_1 in kW	=	11.25	11	10.75	10.75	10.75	10.5	10.5	10.25	10.25
	v_s in mm/min	=						1100 (const.)			
	Δ in mm	=						5 (const.)			

the generation of multi-layer cubes. Due to the continuous heat generation by the electromagnetic stray field, the temperature of the deposited material gradually increased during the printing process. After several layers, the material was fully melted, which resulted in drop formation. Therefore, a parameter adaptation strategy was applied to reduce the temperature during the fabrication of consecutive layers. To this end, P_1 was gradually decreased for each layer until a stable processing strategy was found iteratively through a trial-and-error approach. The test plan according to this procedure is shown in Table 2 as specimen S4.

2.4. Material characterisation

Preparation of LOM cross sections Light optical microscopy (LOM) was used to evaluate the microstructure and defects of printed parts. A Leitz Aristomet light optical microscope with a maximum magnification of 1000 \times was used for this purpose. Sections were mechanically polished and subsequently etched for 90s with 2% NaOH solution.

μ CT image acquisition and analysis An YXLON Precision μ CT was used to record computed tomography (CT) images with an acceleration voltage of 165 kV and a target current of 0.06 mA. 1800 projections were acquired on a 2048 pixel \times 2048 pixel Perkin Elmer XRD1620 AN flat panel detector with a pixel pitch of 200 μ m. For each projection two measurements were recorded with an exposure time of 700 ms and averaged to reduce noise in the projection images. The FDK algorithm with Shepp-Logan filtering in VGStudio MAX 3.4 was used to reconstruct the 3D images with a voxel size of 10.2 μ m.

3. Results and discussion

3.1. Single-layer process window

Fig. 4 shows exemplary single-layer specimens produced with $P_1 = 10$ kW for each type defined in Section 2.3.1. While the type I specimen

(Fig. 4a) shows good shape formation and adhesion between wires, the type I* specimen (Fig. 4b) exhibits only partial adhesion between wires. The shape formation in the type II specimen (Fig. 4c) is also poor. The material is liquid in this process region, leading to drop formation at the reversal points of the path. In contrast, the too low liquid phase fraction of the material in the type III specimen (Fig. 4d) led to the wire breaking into small slices.

Fig. 5 shows the process windows found for $\Delta = 5$ mm (5 a) and for $\Delta = 12$ mm (5 b). In general, semi-solid deposition is feasible by a suitable combination of feed rate and induction power at both inductor-substrate distances. However, no geometrically accurate specimen could be obtained at $\Delta = 12$ mm. It is visible that with increased induction power, the feed rate also has to be increased to produce desirable specimen shapes. When, at a given induction power, the feed rate is too low, fabricated single-layer specimens are overmelted (type II), while too high feed rate leads to breakage of the wire (type III).

The process window at $\Delta = 12$ mm is shifted towards higher feedrate than at $\Delta = 5$ mm. Presumably higher inductor-substrate distances lead to lower coupling of the stray field into the build plate, leaving more heating energy to the wire. Thus higher feed rate is needed to account for the increased energy input. This is similar to the results of Hascoët et al. who also found reduced inductor-substrate distance to increase substrate heating [9]. In addition, a larger inductor-substrate distance increases the time available for heat transfer from the skin of the wire to its core, which can also enable higher feed rates. Inversely, the shape quality of the deposited single-layers significantly deteriorates at $\Delta = 12$ mm (cf. Fig. 4a and b). This is due to the fact that the semi-solid wire is not pushed onto the substrate by means of a nozzle and thus the precision of deposition decreases with greater inductor-substrate distance. In summary, both a semi-solid state of the deposited material and a low inductor-substrate distance are important for proper shape formation.

Fig. 6 shows polished and etched cross-sections of the microstructure of type I, I*, II and III specimens. While the type I and I* specimens

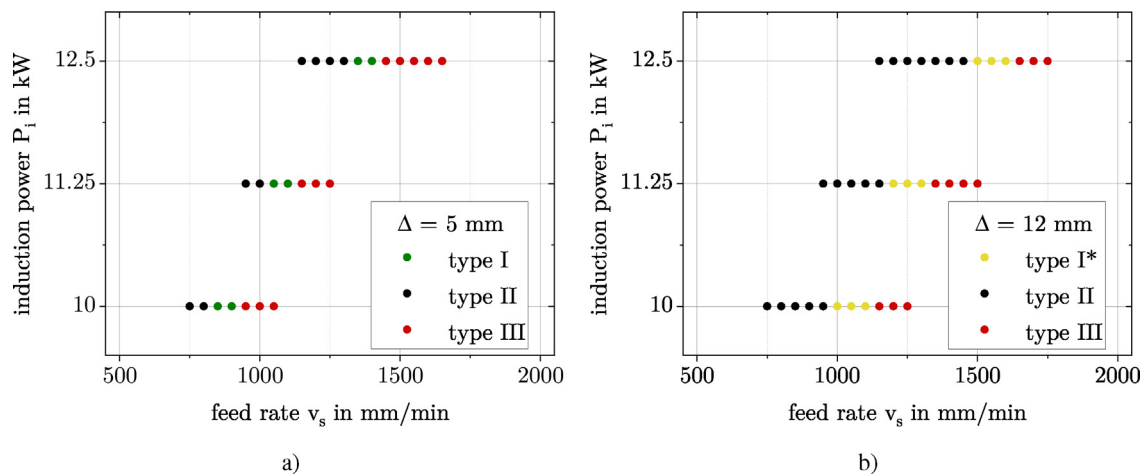


Fig. 5. Process windows of inductive-additive process: a) $\Delta = 5$ mm; b) $\Delta = 12$ mm.

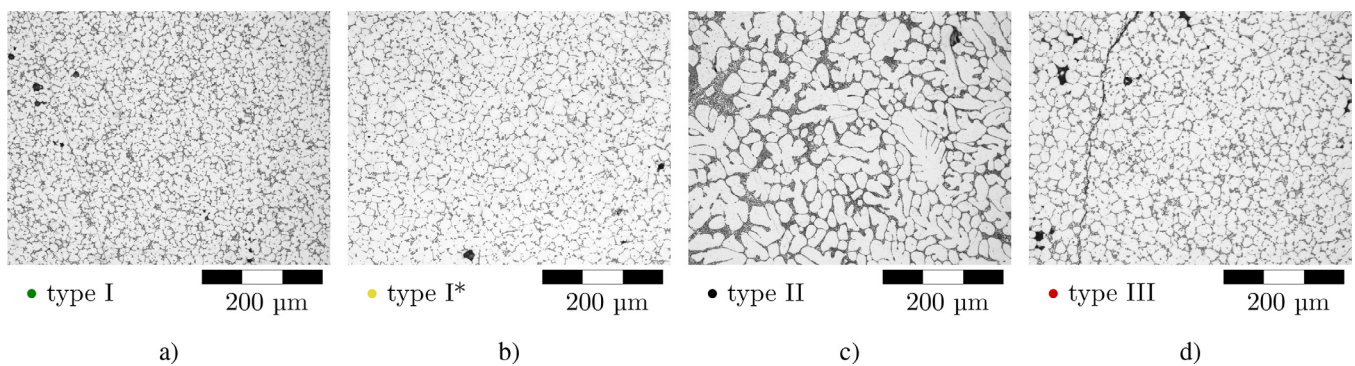


Fig. 6. Microstructure of specimens fabricated: a) inside process window (type I microstructure); b) inside process window (type I* microstructure); c) at too high energy input (type II microstructure); d) at too low energy input (type III microstructure).

show the globular α -Al microstructure typical for semi-solid fabrication processes, the type II specimen shows a microstructure consisting of dendritic α -Al. The microstructure of the type II specimen is the result of the overheating of the wire which is heated beyond the liquidus temperature and then solidifies dendritic. The microstructure in the type III specimen, which is fabricated with too low energy input, is partly similar to type I, but the Si particles (cf. Fig. 1a) did not completely dissolve. Thus the type III microstructure at too low energy input may be the result of too low liquid phase fraction during induction heating in this process region. The higher solid phase fraction in the semi-solid slurry may also explain the larger α -Al particles in the type III and I* microstructures. The higher feed rate possible at 12 mm inductor-substrate distance thus may also in part be caused by the lower shearing of the material needed during deposition and thus lower liquid phase fraction needed.

3.2. Fabrication of multi-layer parts

3.2.1. Cube fabrication strategy

With the results of the single-layer experiments, process strategies for the production of cubes were generated (Table 2: S1, S2 and S3). Only the 5 mm inductor-substrate distance process window was further investigated since the accuracy of the 12 mm inductor-substrate distance produced single-layer specimens was determined to be of inferior quality by visual inspection.

Fig. 7 a–c show cubes which were fabricated with settings from the single-layer process window. A part of the cube fully melted while fabricating the upper layers, because the stray field coupled into the cube.

Thus the processing window from the single-layer experiments seems to be only applicable for the first layer.

Therefore, an adaptation of the processing strategy was investigated. Since the induction generator used in this study allows the induction power to be controlled during operation, the induction power was adapted for each layer using a trial-and-error approach. To this end, the parameter set of S2 was used as a starting point and the induction power was reduced in consecutive layers until fabrication of a cube was possible. When full melting of a part of the cube occurred with a processing strategy, the induction power in the respective layers was decreased. The parameter combination found is shown in Table 2 as specimen S4.

Fig. 7 d shows a cube produced with the adapted strategy exhibiting a reasonable shape. The continuous deposition of the semi-solid wire led to a surface structure similar to that produced by other WFAM processes. The reversal points at the edge of the cube cause accumulation of material due to the slow down of the XYZ-table needed. The utilisation of a linear advance approach or a perimeter - infill build strategy to improve the surface of the specimens is subject to future work.

3.2.2. Microstructure of as-built specimens

To examine the influence of the parameter adaptation over several layers on the microstructure, cross-sections of the multi-layer specimen S4 are shown in Fig. 8. Fig. 8a shows the microstructure of the first layer, while Fig. 8b and c show the microstructure of the middle and last layer, respectively. It is visible that the microstructure shows a distinct variation along the build direction. The first-layer microstructure lost the globular α -Al phase while Si particles formed out of the phase between the globular α -Al, possibly due to the longer time the material stayed heated during fabrication. In contrast, the microstructure in

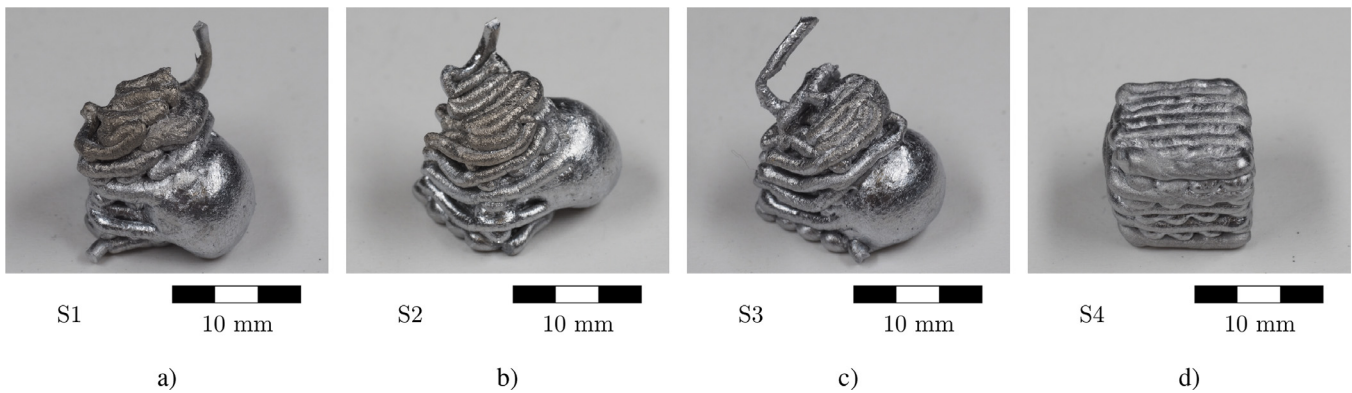


Fig. 7. a) to c): Fabrication results of parameters optimised for single-layer fabrication. Residual heat and the induction stray field led to overmelting of the already deposited material. d): Fabrication result of induction power reduction strategy.

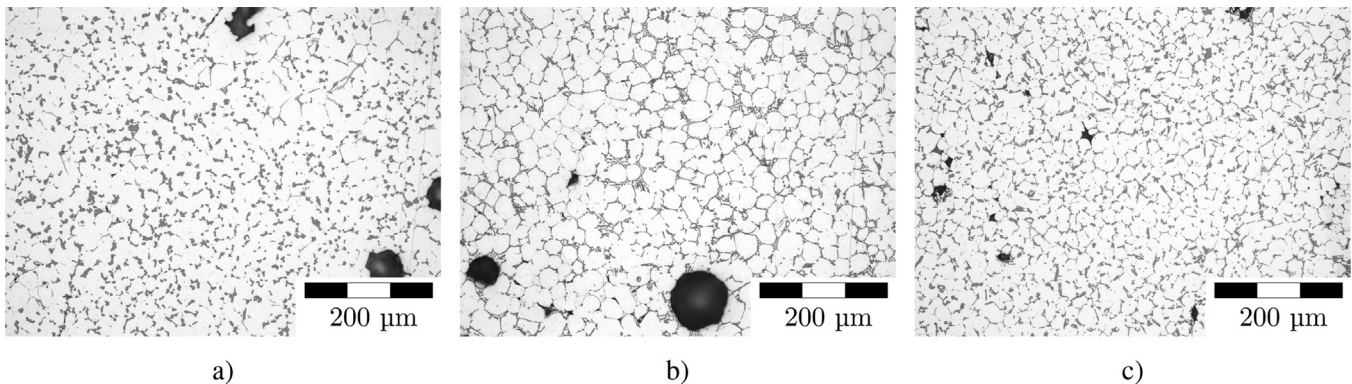


Fig. 8. Cross section images from the first (a)), middle (b)) and last layer (c)) of a cube produced with the induction power variation strategy.

the middle layer (Fig. 8b) is more similar to the microstructure from the single-layer specimens. The last-layer microstructure resembles the type III microstructure. This is probably due to the reduced induction power in the upper layers and the fact that, in contrast to the lower layers, no additional heat was introduced by further deposition of semi-solid material. Further investigations are required to improve the homogeneity of the microstructure through the process parameters or through reduced coupling of the stray field into the already deposited material. Furthermore, a cooling of the deposited material through a directed inert gas stream could reduce the need for parameter adaptation.

Different types of pores can also be seen in Fig. 8. Small pores (between 1 µm and 25 µm diameter) between the globular α -Al are for example visible left in Fig. 8c, while two larger spherical pores (around 50 µm respectively 90 µm diameter) are visible in Fig. 8b. Since the cross sections only show a small area of the sample, μ CT scans are used to analyse the defects in the sample.

3.2.3. Process and feedstock related defects

Fig. 9 shows X-ray CT slice images revealing the defect microstructure of the cube S4 fabricated. The slice image in Fig. 9a shows a plane in build direction of the specimen, while Fig. 9b shows a slice image perpendicular to the build direction. The latter image also shows how the tracks are formed inside the cube. Every track in odd layers is oriented parallel, while the tracks in even layers are perpendicular to the viewing plane. The tracks kept a rounded shape, leaving geometrically induced pores between the tracks. In general, two classes of pores can be distinguished: Spherical porosity and triangular voids between the beads. The diameter of the spherical pores ranges between the resolution limit (10 µm) and around 400 µm. As shown in Fig. 1b, irregular pores exist in the centre of the feedstock wire. As the wire is heated into a semi-solid state during the process, these irregular pores break down

into spherical pores. The origin of the pores in the wire is unknown, it is probably related to the plastic deformation during the production (Mannesmann effect [18]). In future work, different wire feedstocks will be investigated to reduce these defects.

The voids between the beads result from the force-free deposition of the semi-solid wire. This “free” deposition results in an uneven surface of the layer beneath the current layer which can lead to a too high distance between the layers. This is visible between the first and the second layer in Fig. 9b. Moreover, the surface tension and viscosity of the semi-solid metal hinders filling of gaps even with correct inter layer distances, leading to voids between the deposited tracks. Similar voids are known from Fused Filament Fabrication (FFF) processed polymer due to similar mechanisms [21].

4. Conclusion

In the present study, a concept enabling WFAM by means of direct induction heating was presented.

- A narrow process window for the semi-solid processability of wire by means of high frequency induction heating was identified. The process was proven to be able to produce single-layer specimens with build rates of around 20 mm³/s (~0.054 g/s).
- The liquid phase fraction in the deposited material was adjusted by varying the inductor power and feed rate, which affected the shape and microstructure of the specimens.
- Multi-layer parts were feasible after adjusting the process parameters for each layer, i.e. reducing the thermal energy introduced to the wire and the already deposited material. These adjustments changed the liquid phase fraction in the deposited semi-solid material, leading to changes in the microstructure.

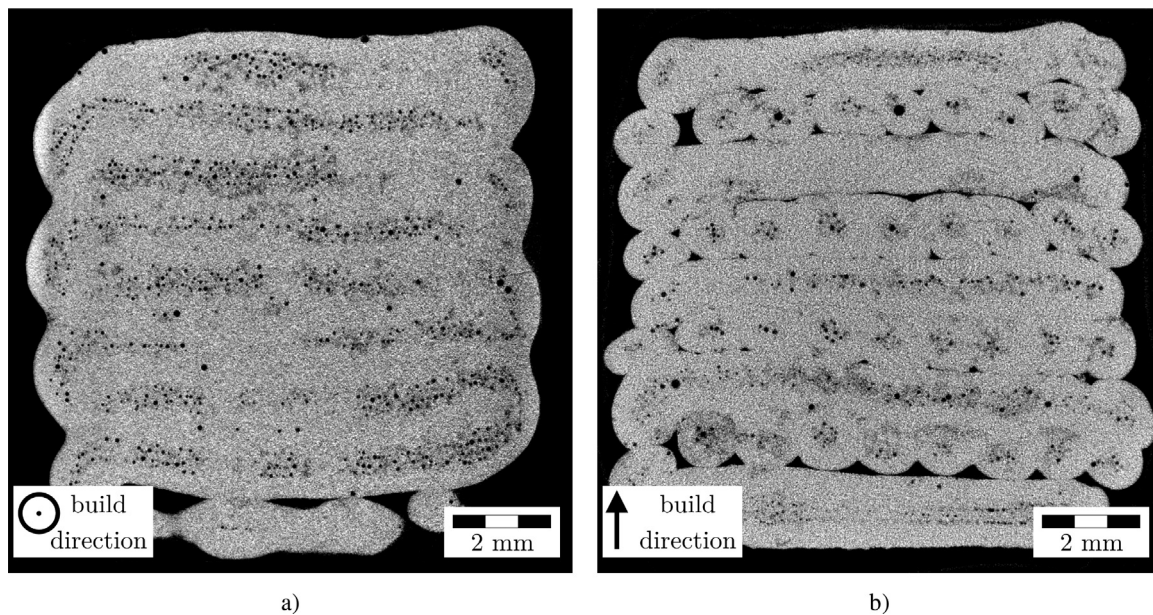


Fig. 9. Defects in specimen S4: a) μ CT slice image perpendicular to build direction (layer 4); b) μ CT slice image in build direction.

- Cubes printed by the process presented here were characterised by means of microstructural analysis and μ CT. The cubes contained feedstock-related defects inside the beads as well as process related defects between the beads similar to FFF materials.

In future studies, attention needs to be focused on process control, for instance by surveillance of the temperature of the semi-solid wire passing the inductor. Furthermore, a spreading of the deposited semi-solid material by a ceramic nozzle may improve the dimensional accuracy and reduce the voids between the beads, similar to fused filament fabrication processes. On the other hand, due to the direct heating of the wire, the novel process without a nozzle could possibly be used advantageously for processing metals with a high melting point.

Declaration of Competing Interest

The authors declare that they have no known competing financial interests or personal relationships that could have appeared to influence the work reported in this paper.

CRediT authorship contribution statement

Lukas Englert: Writing – original draft, Conceptualization, Investigation, Visualization. **Alexander Klumpp:** Conceptualization, Writing – original draft, Investigation. **Antonia Ausländer:** Data curation, Investigation. **Volker Schulze:** Supervision, Writing – review & editing. **Stefan Dietrich:** Conceptualization, Writing – review & editing.

Acknowledgments

The authors thank Moritz Habschied, Simon Höninger and Axel Köhler for their tireless support in the development of the prototype. The research in the “Rolf3D project” did not receive any specific funding from public, commercial or non-profit institutions.

Supplementary material

Supplementary material associated with this article can be found, in the online version, at doi:10.1016/j.addlet.2022.100067.

References

- [1] D. Ding, Z. Pan, D. Cuiuri, H. Li, Wire-feed additive manufacturing of metal components: technologies, developments and future interests, *Int. J. Adv. Manuf. Technol.* 81 (1) (2015) 465–481, doi:10.1007/s00170-015-7077-3.
- [2] M. Tawfik, M. Nemat-Alla, M. Dewidar, Enhancing the properties of aluminum alloys fabricated using wire + arc additive manufacturing technique—A review, *J. Mater. Res. Technol.* (2021), doi:10.1016/j.jmrt.2021.04.076.
- [3] A. Ramalho, T.G. Santos, B. Bevans, Z. Smoqi, P. Rao, J. Oliveira, Effect of contaminations on the acoustic emissions during wire and arc additive manufacturing of 316L stainless steel, *Addit. Manuf.* 51 (2022) 102585, doi:10.1016/j.addma.2021.102585.
- [4] B. Li, L. Wang, B. Wang, D. Li, J. Oliveira, R. Cui, J. Yu, L. Luo, R. Chen, Y. Su, et al., Electron beam freeform fabrication of NiTi shape memory alloys: crystallography, martensitic transformation, and functional response, *Mater. Sci. Eng.* (2022) 143135, doi:10.1016/j.msea.2022.143135.
- [5] J. Oliveira, F.M. Gouveia, T.G. Santos, Micro wire and arc additive manufacturing (μ -WAAM), *Addit. Manuf. Lett.* (2022) 100032, doi:10.1016/j.addlet.2022.100032.
- [6] P. Farahmand, S. Liu, Z. Zhang, R. Kovacevic, Laser cladding assisted by induction heating of Ni-WC composite enhanced by nano-WC and La₂O₃, *Ceram. Int.* 40 (10) (2014) 15421–15438, doi:10.1016/j.ceramint.2014.06.097.
- [7] R. Sun, Y. Shi, X. Wang, Y. Guo, X. Zhou, Investigation of laser assisted ultra-high frequency induction deposition method: processes, fluid flow, and microstructure characteristic, *J. Mater. Res. Technol.* 9 (3) (2020) 2773–2792, doi:10.1016/j.jmrt.2020.01.012.
- [8] R. Sun, Y. Shi, Y. Yang, X. Wang, X. Zhou, Microstructure, element segregation and performance of Inconel 625 metal layer deposited by laser assisted ultra-high frequency induction deposition, *Surf. Coat. Technol.* 405 (2021) 126715, doi:10.1016/j.surfcoat.2020.126715.
- [9] J.-Y. Hascoët, J. Parrot, P. Mognol, E. Willmann, Induction heating in a wire additive manufacturing approach, *Weld. World* 62 (2) (2018) 249–257, doi:10.1007/s40194-017-0533-y.
- [10] G.K. Sharma, P. Pant, P.K. Jain, P.K. Kankar, P. Tandon, On the suitability of induction heating system for metal additive manufacturing, *Proc. Inst. Mech. Eng., Part B* 235 (1–2) (2021) 219–229, doi:10.1177/0954405420937854.
- [11] G.K. Sharma, P. Pant, P.K. Jain, P.K. Kankar, P. Tandon, Analysis of novel induction heating extruder for additive manufacturing using aluminum filament, *Proc. Inst. Mech. Eng., Part B* 235 (12) (2021) 1961–1970, doi:10.1177/09544054211014451.
- [12] S. Semiatin, *Elements of Induction Heating: Design, Control, and Applications*, ASM International, 1988.
- [13] V. Rudnev, D. Loveless, R.L. Cook, *Handbook of Induction Heating*, CRC Press, 2017, doi:10.1201/9781315117485.
- [14] Y. Fei, J. Xu, D. Yao, J. Zhou, From semisolid metal processing to thixotropic 3D printing of metallic alloys, *Virtual Phys. Prototyp.* 0 (0) (2022) 1–19, doi:10.1080/17452759.2022.2045674.
- [15] C.S. Rice, P.F. Mendez, S.B. Brown, Metal solid freeform fabrication using semi-solid slurries, *JOM* 52 (12) (2000) 31–33, doi:10.1007/s11837-000-0065-5.
- [16] A. Jabbari, K. Abrinia, Developing thixo-extrusion process for additive manufacturing of metals in semi-solid state, *J. Manuf. Process.* 35 (2018) 664–671, doi:10.1016/j.jmapro.2018.08.031.

- [17] D.D. Lima, K.N. Campo, S.T. Button, R. Caram, 3D thixo-printing: a novel approach for additive manufacturing of biodegradable Mg-Zn alloys, *Mater. Des.* 196 (2020) 109161, doi:[10.1016/j.matdes.2020.109161](https://doi.org/10.1016/j.matdes.2020.109161).
- [18] J. Gordon, Mannesmann process for making seamless tubes, *RSA J.* 38 (1889) 648.
- [19] M. Habschied, S. Dietrich, D. Heussen, V. Schulze, Performance and properties of an additive manufactured coil for inductive heat treatment in the MHz range, *HTM J. Heat Treat. Mater.* 71 (5) (2016) 212–217, doi:[10.3139/105.110294](https://doi.org/10.3139/105.110294).
- [20] J. Högerl, H. Lipowsky, S. Kroll, H.M. Tensi, Elektrische leitfähigkeit von AlSi7Mg-gußlegierungen/electric conductivity of AlSi7Mg cast alloys, *Int. J. Mater. Res.* 87 (1) (1996) 45–50, doi:[10.1515/ijmr-1996-870108](https://doi.org/10.1515/ijmr-1996-870108).
- [21] Y. Tao, F. Kong, Z. Li, J. Zhang, X. Zhao, Q. Yin, D. Xing, P. Li, A review on voids of 3D printed parts by fused filament fabrication, *J. Mater. Res. Technol.* 15 (2021) 4860–4879.